metals

Article

Phase-Field Modelling of Bimodal Dendritic Solidification During Al Alloy Die Casting

Maryam Torfeh , Zhichao Niu and Hamid Assadi *

Brunel Centre for Advanced Solidification Technology Brunel University London, Uxbridge UB8 3PH, UK; maryam.torfeh@brunel.ac.uk (M.T.); zhichao.niu@brunel.ac.uk (Z.N.)
* Correspondence: hamid.assadi@brunel.ac.uk

Abstract: Tracking the microstructural evolution during high-pressure die casting of Al-Si alloys is challenging due to the rapid solidification, varying thermal conditions, and severe turbulence. The process involves a transition from slower cooling in the shot sleeve to rapid cooling in the die cavity, resulting in a bimodal dendritic microstructure and nucleation of new finer dendrite arms on fragmented externally solidified crystals. In this study, a two-dimensional phase-field model was employed to investigate the solidification behaviour of a hypoeutectic Al-7% Si alloy during high-pressure die casting. The model is based on thermodynamic formulations that account for temperature changes due to phase transformation heat, thermal boundary conditions, and solute diffusion in both liquid and solid phases. To replicate the observed bimodal microstructure, solid–liquid interface properties such as thickness, energy, and mobility were systematically varied to reflect the transition from the shot sleeve to the die cavity. The results demonstrated the model's ability to capture the growth of dendrites under shot sleeve conditions and nucleation and development of new dendrite arms under the rapid cooling conditions of the die cavity.

Keywords: phase-field modelling; HPDC; interface behaviour

check for updates

Academic Editors: Hélder Puga, Heinz-Günter Brokmeier, Alain Pasturel, Rongshan Qin and Oleg Mishin

Received: 29 November 2024
Revised: 3 January 2025
Accepted: 9 January 2025
Published: 13 January 2025

Citation: Torfeh, M.; Niu, Z.; Assadi, H. Phase-Field Modelling of Bimodal Dendritic Solidification During Al Alloy Die Casting. *Metals* **2025**, *15*, 66. https://doi.org/10.3390/met15010066

1. Introduction

High-pressure die casting (HPDC) is an economical method for manufacturing near-net shape lightweight aluminium alloys. Several factors during HPDC can fundamentally influence the final quality of the product. Process factors such as intensification pressure, plunger speed, and die temperature have been studied by many researchers [1–3]. The cooling rate in HPDC in the shot sleeve is about 100 K/s, while in the die is about 1000 K/s [4,5]. The microstructure of the final components is not just dependent on the cooling rate. The severe shearing and turbulence during the injection stage remarkably affect the microstructure.

The solidification condition in the shot sleeve is very close to simple gravity casting. Helenius et al. [6], studying the melt heat transfer while entering the shot sleeve, defined four zones with distinct heat transfer coefficients and turbulence. The temperature of Al-7% Si melt in the shot sleeve has been reported to be about 620 °C [3,6], which is very close to the liquidus temperature of the alloy. In HPDC, the metal flow rate exceeds the solid–liquid interface velocity. Primary dendrites initiate formation in the shot sleeve, and due to the rapid solidification and high metal velocity, columnar dendrites cannot develop within the thin channels, resulting in a non-dendritic structure. Such microstructural features significantly influence the as-cast properties of the castings. One of the most frequently reported microstructural issues in the HPDC of aluminium alloys is the presence of externally solidified crystals (ESCs) in the final product. These crystals are formed before entering the die and have much growth time. Ji et al. [7] evaluated the size distribution of the α-Al phase in the shot sleeve and die, revealing that ESCs nucleate in the shot sleeve before the melt is injected into the die. Studies have shown that coarse ESCs in the final microstructure significantly affect mechanical properties [8]. Efforts to control ESCs by altering process parameters [9] or modifying chemical composition [10–12] have demonstrated substantial impacts on mechanical properties. The effect of microstructure on mechanical properties is more pronounced in large components manufactured by HPDC, where the high flow length makes it challenging to control the uniformity of the microstructure. Niu et al. [3] have reported variations in yield strength, ultimate tensile strength, and elongation along the flow length of large HPDC components.

Although controlling the microstructure is crucial for achieving uniform mechanical properties, it is challenging to accomplish in fast-paced processes like high-pressure die casting (HPDC). Given the difficulties in tracking the solidification trend in HPDC, employing numerical simulations has proven to be a more efficient approach for optimising casting design and process parameters [6,13]. Several studies have applied various numerical methods to better understand the processes during HPDC. Most of these studies focus on fluid dynamics and heat transfer modelling using the Finite Element Method (FEM). For instance, El-Mahallawy et al. [14] applied a 2D heat-flow model to study the effects of pressure variations and fluid velocity at the in-gate on temperature distribution. Kwon et al. [15] simulated the filling process to optimise the runner systems and predict shrinkage areas. There have also been a few studies that have attempted to go one step further and predict microstructure evolution. These studies typically simulate heat transfer and fluid flow using FEM and then combine the results with Cellular Automata (CA) to predict the grain size of the final casting [13,16,17]. The phase-field method is widely used for modelling the evolution of the liquid/solid interface during solidification, where a diffuse interface with a hypothetical thickness helps to smoothly track transitions between phases. However, it has rarely been used for modelling HPDC. The aim of this study is to analyse dendritic structure evolution during HPDC and provide insights into how rapid solidification leads to the formation of bimodal dendritic arms.

2. Materials and Methods

The alloy used in this study was a hypo-eutectic Al-Si alloy with a chemical composition given in Table 1. The casting had been produced by a 16,000 KN cold chamber HPDC machine, for which the process parameters were discussed elsewhere [3].

Table 1. Chemical composition of hypo-eutectic Al-Si alloy.

Elements	Si	Mg	Mn	Fe	Ti	Cu	Sr	Al
Wt%	6.70	0.20	0.51	0.07	0.07	0.01	0.012	Bal.

2.1. Microstructure Study

The casting was a ribbed plate of 700 mm × 220 mm × 2.8 mm, connected to a four-channel gating system, Figure 1. The microstructure was evaluated on the cross-section of the samples from different locations along the plate. The samples were prepared for optical microscopy, grinding with SiC abrasive papers, and polishing with an Al_2O_3 suspension. The samples were then anodised and studied using a Zeiss Axio-Vision optical microscope for microstructure observation.

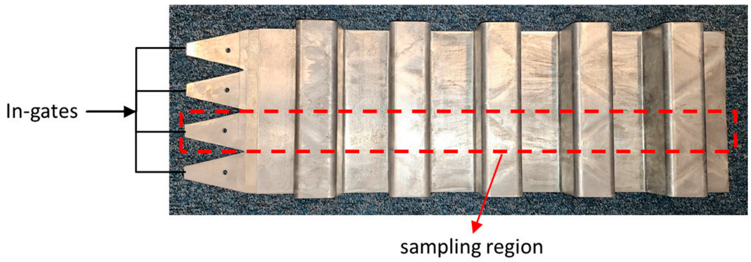

Figure 1. Sampling region on the plate manufactured by HPDC.

2.2. Numerical Study

2.2.1. Phase-Field Model

The main idea of the phase-field method is to introduce a diffuse interface by a Cahn–Hilliard type equation to define the local free energy density at the interface [18]. An order parameter, $\varnothing$, defines the interface transition by varying between 0 and 1 moving from liquid to solid, respectively. C and T represent composition and temperature. The overall free energy (F) of the system can be calculated through the following equations.

$$F = \int \left[f\left(\varnothing,\ x_{Si}^{L},\ x_{Si}^{S},\ T\right) + \frac{1}{2}\varepsilon^2 |\nabla\varnothing|^2 + g(\theta) \right] dV \quad (1)$$

$$f = h_1 F_s + (1 - h_1) F_L + h_2 W \quad (2)$$

where f represents the local volumetric free energy density which is a function of free energies of solid and liquid phases (F_S and F_L), the energy barrier separating two phases (W), and $\varnothing$-related functions, h_1 and h_2. Additionally, ε is a constant associated with the thickness of the solid/liquid interface, and $g(\theta)$ accounts for the free energy arising from the crystallographic misorientation of neighbouring cells.

The temperature and composition fields need to be calculated separately and fed into Equation (1). The temperature field is calculated according to Equation (3).

$$\frac{\partial T}{\partial t} = \alpha_{th} \nabla^2 T + \frac{1}{C_p} \frac{\partial H_{tr}}{\partial t} \quad (3)$$

where α_{th} is the thermal diffusivity, and C_p is the average heat capacity. The first term identifies how external heating/cooling affects the temperature distribution in the system, and the second term yields the effects of phase transformation on the temperature field. H_{tr} represents the enthalpy of transformation that is derived from the Gibbs–Helmholtz equation as follows

$$H_{tr} = (1 - h_1) G_{ex}^{L} + h_1 \left(G_{ex}^{S} - L \right) \quad (4)$$

where $L = (1 - x_{Si}) L_{Al} + x_{Si} L_{Si}$ is the average latent heat of fusion of the constituents, and G_{ex}^{L} and G_{ex}^{S} are the excess free energies of the liquid and solid phases, respectively.

The evolution of the composition field is coupled to the phase-field parameter, $\varnothing$, which tracks the interface between solid and liquid. The difference in diffusivity between the solid and liquid phases influences how elements redistribute themselves during solidification. On the other hand, the composition field affects the local driving force for phase transformation and thus influences the evolution of $\varnothing$. The free energy functional couples all the variables, dictating how the system's microstructure evolves during solidification.

2.2.2. Domain and Boundary Conditions

A two-step process was defined for simulating solidification in HPDC, reflecting the conditions in the shot sleeve and the die. Two-dimensional simulations were performed on a grid of 500 × 500 cells. The composition of the liquid phase was set to Al-7 Wt% Si, while the initial solid nuclei were assumed to contain 1 Wt% Si. Material properties and model parameters are summarised in Table 2. Additionally, the boundary conditions for solidification in the shot sleeve and the die are provided in Table 3.

Table 2. Material properties and model parameters.

Parameter			Value
Material properties	Melting temperatures	Tm (Al)	933.50 K
		Tm (Si)	1687.15 K
	Latent heat	L (Al)	1050×10^6 J/m^3
		L (Si)	4194×10^6 J/m^3
	Heat capacity	Cp (Al)	2.4×10^6 J/K.m^3
		Cp (Si)	1.7×10^6 J/K.m^3
Model parameters	Interaction parameters	Ω_{solid}	28,000 J/mol
		Ω_{liquid}	−8000 J/mol
	S/L interface thickness	Δx (Shot sleeve)	700 nm
		Δx (Die)	500, 600, 700 nm
	S/L interface energy	E (Shot sleeve)	0.16 J/m^2
		E (Die)	0.10, 0.16, 0.20 J/m^2
	S/L interface mobility	μ (Shot sleeve)	0.003 m/sK
		μ (Die)	0.001, 0.003, 0.009 m/sK

Table 3. Thermal boundary conditions.

Process Parameter	Shot Sleeve	Die Cavity
Initial temperature	650 K	450 K
Cooling rate	100 K/s	1000 K/s

3. Results

3.1. Microscopic Observations

The microstructure of the plate comprised the α-Al phase, the Al-Si eutectic phase, and a small fraction of intermetallic phases (less than 1 vol.%), which can be neglected in solidification modelling [19,20]. In each section examined, the characteristic regions of high-pressure die-cast structures were identified, including the central area, the outer skin, and the segregation band, as illustrated in Figure 2. A progressive change in microstructure was observed when moving from the in-gate towards the end of the plate. Specifically, the average α-Al particle size exhibited a significant reduction, decreasing from approximately 21 μm near the in-gate of the die (sample 1) to approximately 3 μm at the far end of the plate (sample 7).

Additionally, the segregation band became increasingly prominent starting from sample 6 and extending towards the end of the casting. This feature indicates a variation in solute distribution, likely influenced by the local solidification front behaviour and flow characteristics during the casting process. The presence and evolution of these structural features provide valuable insight into the solidification mechanisms and the influence of casting parameters on the final microstructure.

The distribution of the α-Al particles at three distinct positions along the length of the plate was evaluated and presented in Figure 3. The analysis results indicate a noticeably higher fraction of large α-Al particles near the in-gate region of the casting, with their quantity decreasing significantly as the observation point moves towards the end of the casting. Approximately 70% of the α-Al particles in the middle section of the plate and beyond fall within the size range of 0–10 μm, indicating a finer and more uniform particle distribution in these areas.

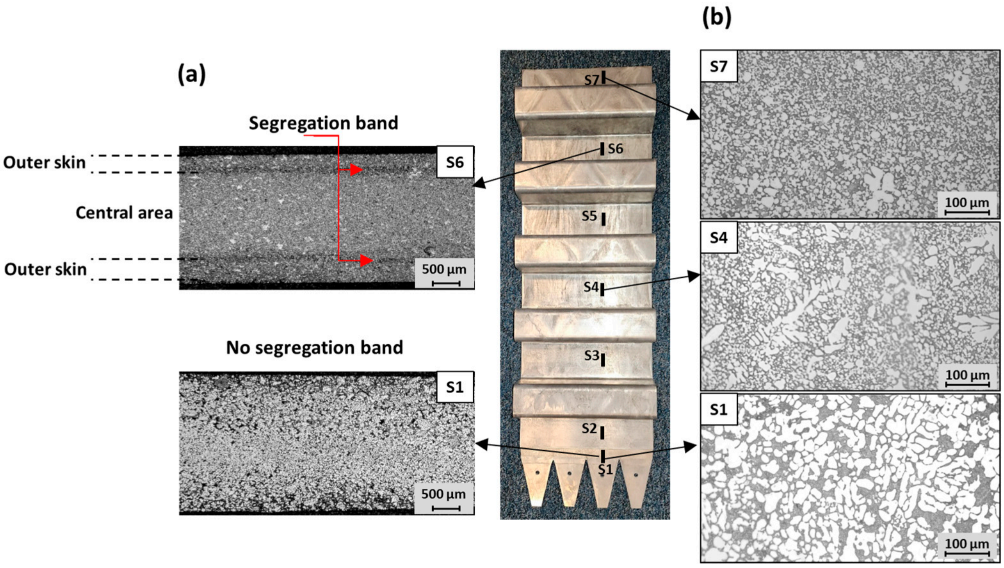

Figure 2. Microstructure evolution at seven sampling locations (S1-S7) along the plate, (**a**) advent of segregation band at last one-third of the plate shown by red arrows, (**b**) comparison of α-Al particles.

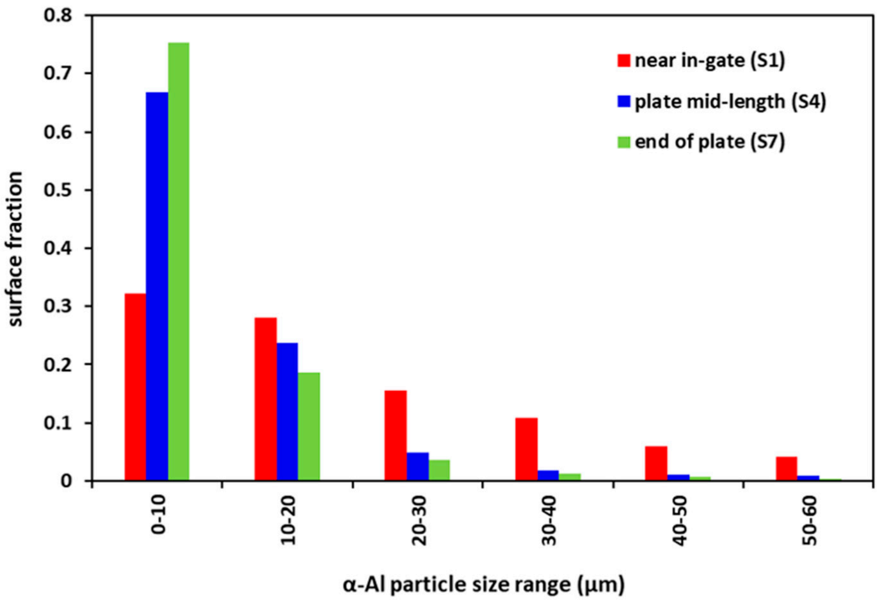

Figure 3. Size distribution of α-Al particles along the plate.

Upon comparing the micrographs of α-Al particles at the in-gate and the furthest area of the plate from the in-gate, as shown in Figure 4a, a distinct accumulation of fine α-Al particles between the large ESCs can be observed at the beginning of the plate, immediately after passing through the in-gate. This region demonstrates the coexistence of fine, dispersed α-Al particles surrounding the larger ESCs, contributing to a heterogeneous microstructure. Additionally, new arms were observed nucleating on the fragmented dendrites, as indicated by the arrows in Figure 4b, which provides a higher magnification view for clarity. By contrast, at the end of the plate, shown in Figure 4c, only a limited number of ESCs were detected. The α-Al particles in the central area of this region appeared significantly finer and more uniformly distributed compared to the earlier sections of the plate, further emphasising the variation in solidification dynamics across the casting length.

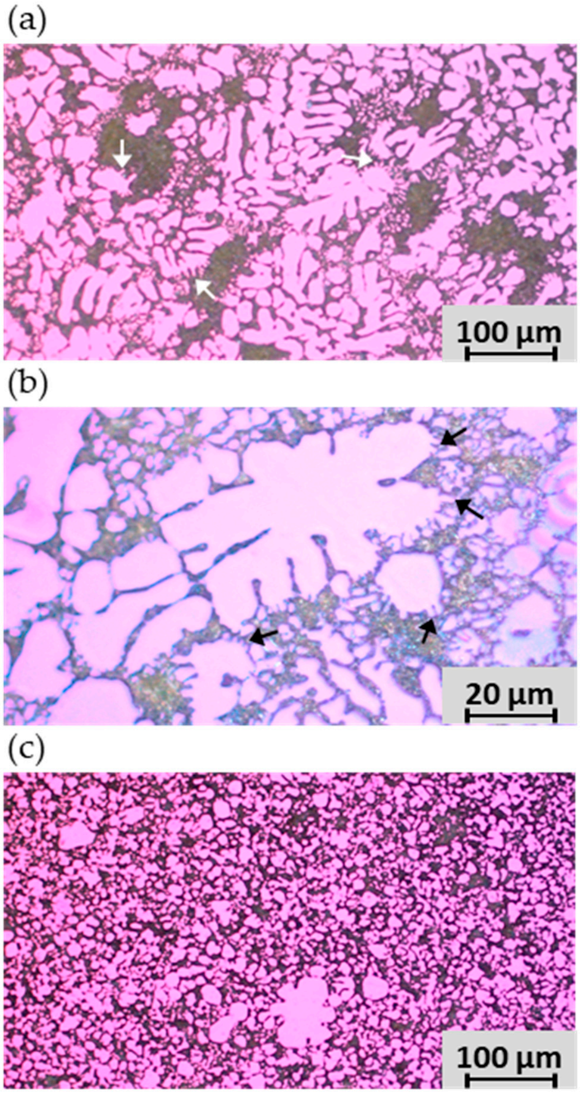

Figure 4. Comparison of α-Al particles along the plate, (**a**) and (**b**) near the in-gate, (**c**) at the end of the plate (the arrows show the new arms nucleated on fragmented dendrites).

3.2. Numerical Results

3.2.1. Simulation of Dendritic Growth in the Shot Sleeve

Considering the high manufacturing rate of the HPDC process, the melt remains in the shot sleeve for a short time resulting in limited formation of primary dendrites. The solidification condition at the HPDC shot sleeve before injection has been shown to be very similar to the gravity die casting [21]. The microstructure at the in-gate was used to calibrate the simulation since the fraction of the ESCs is at the maximum amount at the beginning of the plate. Although the shape of the dendrites can change during injection due to fragmentation, it was assumed that the size of dendrite arms after the in-gate is still comparable with the dendrites' sizes in the shot sleeve. An optical microscopy image of the microstructure immediately after the in-gate has been provided in Figure 5a. A 500 µm × 500 µm domain with an initial nucleation fraction of 0.001 was introduced. The seeds were randomly oriented and grown at the shot sleeve condition for a duration of 2 ms. Under these conditions, dendritic growth was characterised by the elongation and thickening of primary and secondary arms, consistent with the controlled cooling and thermal gradients. The S/L interface properties—thickness (700 nm), energy (0.16 J/m), and mobility (0.003 m/sK)—were sufficient to replicate the growth observed during this phase, Figure 5b,c.

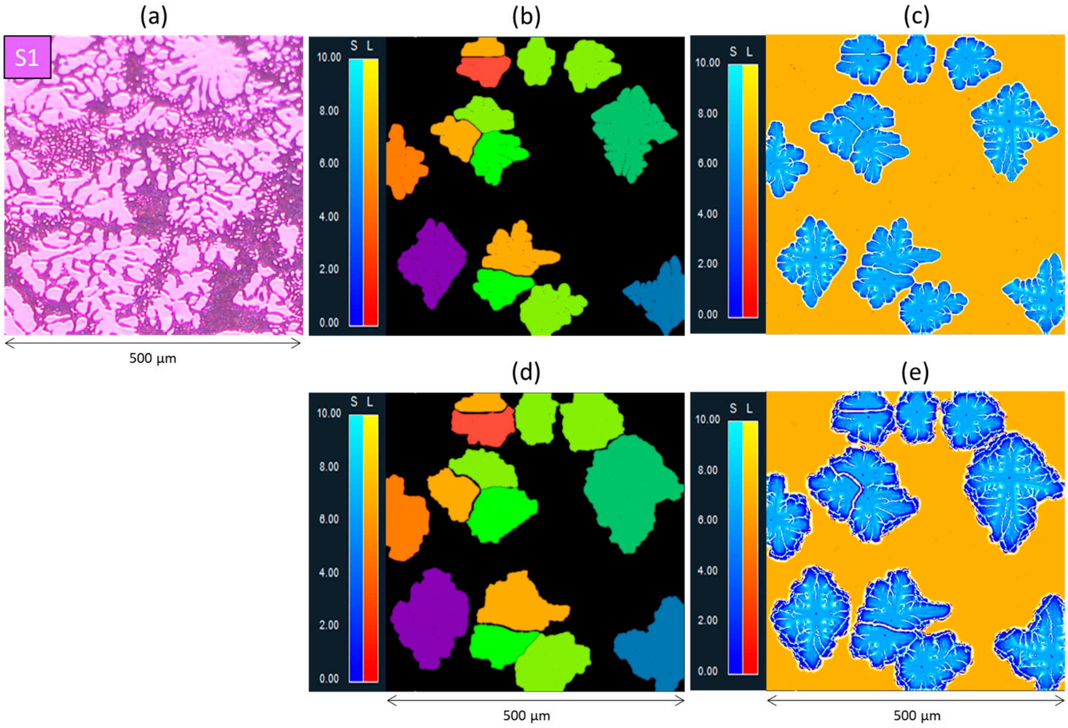

Figure 5. (**a**) Externally solidified crystals at the in-gate, (**b**,**c**) phase-field and Si concentration of dendrites at shot sleeve after 2 ms, (**d**,**e**) after 15 ms.

3.2.2. Transition to Die Cavity Conditions

The solidification process in the die cavity was modelled with a focus on the nucleation of new dendrite arms on a single externally solidified crystal under new rapid solidification conditions, as illustrated in Figure 6. After 2 ms of growth, the simulation parameters were adjusted to represent the rapid solidification conditions within the die cavity more accurately. Specifically, the cooling rate was increased to 1000 K/s, the initial temperature was reduced to 450 K, and the temperature gradient was set to zero to simulate a more uniform thermal environment. The properties of the solid–liquid (S/L) interface were systematically varied to assess their impact on dendritic morphology, with the conditions summarised in Table 4.

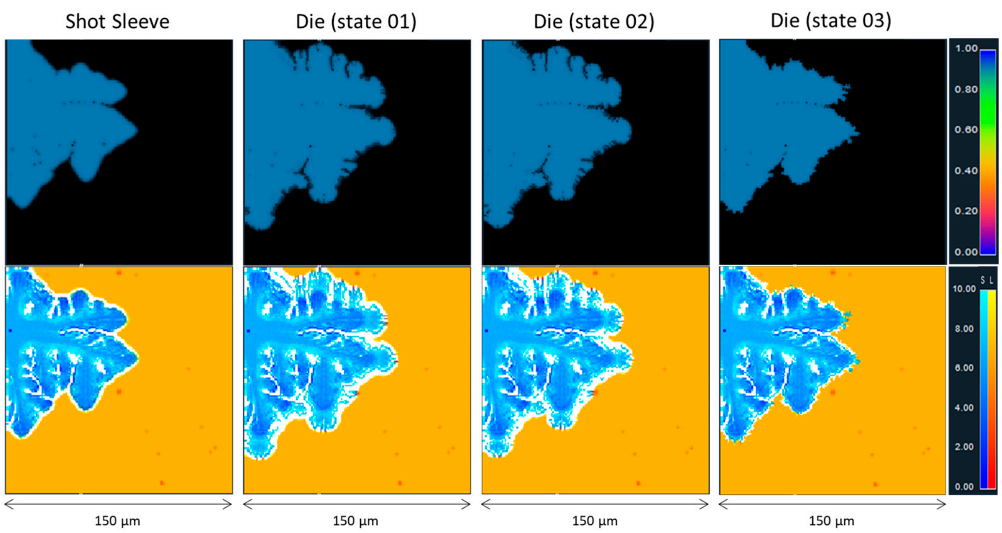

Figure 6. Comparison of secondary nucleation on a dendrite grew in the shot sleeve for 2 ms and transferred to die cavity (states 1–3 show interface thicknesses of 700–500 nm).

Table 4. Modelling plan with variable model parameters.

State No.	Solid/Liquid Interface Thickness (nm)	Interface Energy (J/m^2)	Interface Mobility (m/sK)
01	700	0.160	0.003
02	600	0.160	0.003
03	500	0.160	0.003
04	700	0.100	0.003
05	700	0.200	0.003
06	700	0.160	0.001
07	700	0.160	0.009

4. Discussion

The distribution of α-Al particles in the casting attracts attention from two perspectives. Firstly, moving away from the in-gate along the plate, the average size of the particles noticeably reduced. The large externally solidified crystals (ESCs) [6,22–26] were nucleated in the shot sleeve and were forced into the die through the injection. The morphology of these particles shows blunted dendrite arms, resulting from the shearing and fragmentation of dendrites as they pass through the die in-gate at speeds as high as 50 m/s [3,27].

The second point of interest is the size segregation of α-Al particles which causes the particles to distribute radially, with larger particles moving toward the centre of the flow while smaller particles remain near the walls. Size segregation during HPDC has been evaluated in several studies and can be influenced by various parameters affecting the drag forces of the fluid and particle shearing. For instance, changing the melt superheat has been shown to alter the microstructure, making it more dendritic or more globular, with a noticeable effect on shearing and segregation [28]. The segregation band, which contains a high amount of Al-Si eutectic, appears in different thicknesses and distances from the wall depending on the Si concentration and externally solidified crystals fraction in the alloy [29]. The pressure of the molten metal tends to drop as it flows through the die. The flow may transition from more turbulent near the gate to more laminar as it reaches the end of the plate. Turbulent flow in the initial sections can enhance mixing and reduce the likelihood of segregation. As the flow becomes more laminar, solutes may have more opportunity to separate, contributing to segregation in the later stages of solidification. Overall, the lower fraction of ESCs, reduced melt pressure, and less turbulence in the flow can explain the formation of the segregation band in the last third of the plate length.

Turbulence in the die cavity disrupts the solute boundary layer and enhances localised undercooling, facilitating the nucleation of tertiary dendrite arms. A reduction in S/L interface thickness from 700 nm to 500 nm improved the simulation’s ability to capture this behaviour. A thinner interface represents sharper gradients, consistent with the enhanced heat and solute transfer caused by turbulence. This adjustment enabled the model to accurately depict the finer dendritic features observed in experimental microstructures.

Varying the interface energy altered the driving force for dendrite growth and tip stability. Increasing the interface energy to 0.20 J/m suppressed tip branching, likely due to reduced thermal fluctuations at the interface, which could have dampened the turbulence-induced effects. Conversely, lowering the interface energy to 0.10 J/m caused excessive tip branching, leading to unrealistically irregular structures.

Interface mobility governs the rate at which the solid–liquid interface advances, influenced by local temperature and solute conditions. In turbulent environments, enhanced mixing increases the effective cooling rate and accelerates dendrite growth. The moderate interface mobility of 0.003 m/sK matched the observed tertiary arm sizes, reflecting the interplay between rapid cooling and turbulence-enhanced solute transport. Reducing mobility to 0.001 m/sK resulted in slower dendrite growth while increasing it to 0.009 m/sK led to exaggerated arm elongation, inconsistent with experimental microstructures.

Although this phase-field model primarily focused on solidification, the physical effects of turbulence can be inferred indirectly through the change in solid–liquid interface thickness. The turbulence accelerates heat extraction, which is reflected in the thinner interface during solidification in the die cavity. This sharper interface indicates a more rapid transition from liquid to solid, as might be expected under turbulent flow conditions where cooling rates are elevated. The turbulence-related fragmentation and increased local undercooling promote secondary nucleation on pre-existing dendrites, which has been successfully captured in this phase-field simulation.

5. Conclusions

Turbulence-induced fragmentation is a critical factor in modifying dendrite morphology during the high-pressure die casting (HPDC) of Al-Si alloys. The high-velocity melt transfer from the shot sleeve to the die cavity promotes the fragmentation of secondary dendrite arms, which subsequently act as nuclei for the growth of new arms. These phenomena are particularly pronounced in regions with elevated solute and thermal gradients, where turbulence enhances localised undercooling and solute redistribution.

The phase-field modelling approach successfully captured the initiation and growth of new dendrite arms by systematically varying solid–liquid interface properties. The selected parameter set effectively represented the morphological changes induced by turbulence and rapid cooling in the die cavity by reducing interface thickness. This highlights the interplay between kinetic and thermodynamic factors in dendrite evolution under HPDC conditions.

These findings provide critical insights into the role of turbulence in dendritic solidification and demonstrate the utility of phase-field modelling in replicating complex microstructural phenomena. The results also underscore the importance of tuning interface properties to account for process-specific conditions, offering a pathway for further optimisation of HPDC processes and microstructural control in Al-Si alloys.

Author Contributions: Conceptualization, M.T. and H.A.; Methodology, M.T. and H.A.; Software, M.T.; Validation, M.T. and Z.N.; Investigation, M.T.; Writing—Original Draft Preparation, M.T.; Writing—Review and Editing, Z.N. and H.A.; Visualisation, M.T.; Supervision, H.A. All authors have read and agreed to the published version of the manuscript.

Funding: This research was funded by the EPSRC (EP/V061798/1) through the Materials Made Smarter Research Centre.

Data Availability Statement: The original contributions presented in this study are included in the article. Further inquiries can be directed to the corresponding author.

Acknowledgments: The authors gratefully acknowledge Shouxun Ji for his valuable advice and the EPSRC for funding the Materials Made Smarter Research Centre.

Conflicts of Interest: The authors declare no conflicts of interest. The funders had no role in the design of the study; in the collection, analyses, or interpretation of data; in the writing of the manuscript; or in the decision to publish the results.

References

1. Han, Q.; Zhang, J. Fluidity of Alloys Under High-Pressure Die Casting Conditions: Flow-Choking Mechanisms. *Metall. Mater. Trans. B* **2020**, *51*, 1795–1804. [CrossRef]
2. Mednanský, M.; Bruna, M.; Matejka, M. Electromotor Housing Microstructure Dependence on HPDC Process Parameters. *Transp. Res. Procedia* **2023**, *74*, 680–687. [CrossRef]
3. Niu, Z.; Liu, G.; Li, T.; Ji, S. Effect of High Pressure Die Casting on the Castability, Defects, and Mechanical Properties of Aluminium Alloys in Extra-Large Thin-Wall Castings. *J. Mater. Process. Technol.* **2022**, *303*, 117525. [CrossRef]
4. Zhu, X.; Dong, X.; Blake, P.; Ji, S. Improvement in As-Cast Strength of High-Pressure Die-Cast Al–Si–Cu–Mg Alloys by Synergistic Effect of Q-$Al_5Cu_2Mg_8Si_6$ and θ-Al_2Cu Phases. *Mater. Sci. Eng. A* **2021**, *802*, 140612. [CrossRef]
5. Laukli, H.I.; Gourlay, C.M.; Dahle, A.K.; Lohne, O. Effects of Si Content on Defect Band Formation in Hypoeutectic Al-Si Die Castings. *Mater. Sci. Eng. A* **2005**, *413–414*, 92–97. [CrossRef]
6. Helenius, R.; Lohne, O.; Arnberg, L.; Laukli, H.I. The Heat Transfer during Filling of a High-Pressure Die-Casting Shot Sleeve. *Mater. Sci. Eng. A* **2005**, *413*, 52–55. [CrossRef]
7. Ji, S.; Wang, Y.; Watson, D.; Fan, Z. Microstructural Characteristics of Diecast AlMgSiMn Alloy. *Mater. Sci. Forum* **2014**, *783*, 234–239. [CrossRef]
8. Zheng, H.; Jiang, Y.; Liu, F.; Zhao, H. Synergistic Effect of Externally Solidified Crystals and Fe-Rich Intermetallic on the Fracture Behavior of HPDC Alloy. *J. Mater. Res. Technol.* **2023**, *27*, 2822–2832. [CrossRef]
9. Xie, H.; Wang, J.; Li, Y.; Song, J.; Hu, H.; Qin, L.; Zhao, H.; Li, C.; Cui, Y.; Tan, Z.; et al. Fast Shot Speed Induced Microstructure and Mechanical Property Evolution of High-Pressure Die Casting Mg-Al-Zn-RE Alloys. *J. Mater. Process. Technol.* **2024**, *331*, 118523. [CrossRef]
10. Li, J.; Yu, W.; Sun, Z.; Zheng, W.; Zhang, L.; Xue, Y.; Liu, W.; Xiong, S. Influence of Introducing Zr, Ti, Nb and Ce Elements on Externally Solidified Crystals and Mechanical Properties of High-Pressure Die-Casting Al–Si Alloy. *Int. J. Miner. Metall. Mater.* **2025**, *32*, 147–153. [CrossRef]
11. Zhu, X.; Yang, H.; Dong, X.; Ji, S. The Effects of Varying Mg and Si Levels on the Microstructural Inhomogeneity and Eutectic Mg2Si Morphology in Die-Cast Al–Mg–Si Alloys. *J. Mater. Sci.* **2019**, *54*, 5773–5787. [CrossRef]
12. Yang, Q.; Wu, X.; Qiu, X. Microstructural Characteristics of High-Pressure Die Casting with High Strength–Ductility Synergy Properties: A Review. *Materials* **2023**, *16*, 1954. [CrossRef] [PubMed]
13. Gu, C.; Lu, Y.; Cinkilic, E.; Miao, J.; Klarner, A.; Yan, X.; Luo, A.A. Predicting Grain Structure in High-Pressure Die Casting of Aluminum Alloys: A Coupled Cellular Automaton and Process Model. *Comput. Mater. Sci.* **2019**, *161*, 64–75. [CrossRef]
14. El-Mahallawy, N.A.; Taha, M.A.; Pokora, E.; Klein, F. On the influence of process variables on the thermal conditions and properties of high pressure die-cast magnesium alloys. *J. Mater. Process. Technol.* **1998**, *73*, 125–138. [CrossRef]
15. Kwon, H.J.; Kwon, H.K. Computer aided engineering (CAE) simulation for the design optimization of gate system on high pressure die casting (HPDC) process. *Robot. Comput.-Integr. Manuf.* **2019**, *55*, 147–153. [CrossRef]
16. Sharifi, P.; Jamali, J.; Sadayappan, K.; Wood, J.T. Grain size distribution and interfacial heat transfer coefficient during solidification of magnesium alloys using high pressure die casting process. *J. Mater. Sci. Technol.* **2018**, *34*, 324–334. [CrossRef]
17. Dou, K.; Lordan, E.; Zhang, Y.J.; Jacot, A.; Fan, Z.Y. A complete computer aided engineering (CAE) modelling and optimization of high pressure die casting (HPDC) process. *J. Manuf. Process.* **2020**, *60*, 435–446. [CrossRef]
18. Assadi, H. A Phase-Field Model for Non-Equilibrium Solidification of Intermetallics. *Acta Mater.* **2007**, *55*, 5225–5235. [CrossRef]
19. Li, B.; Xu, Q.Y.; Liu, B.C. Numerical Modeling of Microstructure Evolution and Dendrite Growth for Al-Si Alloy Casting during Low Pressure Die Casting. *Mater. Sci. Forum* **2007**, *561–565*, 1787–1792. [CrossRef]
20. Belov, N.A.; Eskin, D.G.; Aksenov, A.A. *Multicomponent Phase Diagrams: Applications for Commercial Aluminum Alloys*; Elsevier: Amsterdam, The Netherlands, 2005; p. 48.
21. Dey, A.K.; Poddar, P.; Singh, K.K.; Sahoo, K.L. Mechanical and Wear Properties of Rheocast and Conventional Gravity Die Cast A356 Alloy. *Mater. Sci. Eng. A* **2006**, *435–436*, 521–529. [CrossRef]
22. Zheng, H.; Jiang, Y.; Liu, F.; Zhao, H. Microstructure Heterogeneity Optimization of HPDC Al-Si-Mg-Cu Alloys by Modifying the Characteristic of Externally Solidified Crystals. *J. Alloys Compd.* **2024**, *976*, 173167. [CrossRef]
23. Otarawanna, S.; Gourlay, C.M.; Laukli, H.I.; Dahle, A.K. Microstructure Formation in High Pressure Die Casting. *Trans. Indian Inst. Met.* **2009**, *62*, 499–503. [CrossRef]
24. Laukli, H.I.; Gourlay, C.M.; Dahle, A.K. Migration of Crystals during the Filling of Semi-Solid Castings. *Metall. Mater. Trans. A* **2005**, *36*, 805–818. [CrossRef]
25. Hao, Y.Z.; Zhao, H.D.; Shen, X.; Wang, X.L.; Zheng, H.T. Simulation of α-Al Grain Formation in High Vacuum Die-Casting Al-Si-Mg Alloys with Multi-Component Quantitative Cellular Automaton Method. *China Foundry* **2022**, *19*, 99–108. [CrossRef]
26. Han, Q.; Xu, H. Fluidity of Alloys under High Pressure Die Casting Conditions. *Scr. Mater.* **2005**, *53*, 7–10. [CrossRef]

27. Reyes, A.E.S.; Guerrero, G.A.; Ortiz, G.R.; Gasga, J.R.; Robledo, J.F.G.; Flores, O.L.; Costa, P.S. Microstructural, Microscratch and Nanohardness Mechanical Characterization of Secondary Commercial HPDC AlSi9Cu3-Type Alloy. *J. Mater. Res. Technol.* **2020**, *9*, 8266–8282. [CrossRef]
28. Zhang, H.; Li, D.; Wang, Q.; Fan, Z.; Luo, M.; Midson, S.P.; Zhu, Q. Effect of Primary α-Al Morphology in Slurry on Segregation during 357 Semi-Solid Die Casting. *Solid State Phenom.* **2019**, *285*, 398–402. [CrossRef]
29. Gourlay, C.M.; Laukli, H.I.; Dahle, A.K. Segregation Band Formation in Al-Si Die Castings. *Metall. Mater. Trans. A* **2004**, *35*, 2881–2891. [CrossRef]